ARTICLE WILEY-VCH

Structural reversibility of $LaCo_{1-x}Cu_xO_3$ followed by in situ X-ray diffraction and absorption spectroscopy

Rosa Pereñíguez*[a] and Davide Ferri [b]

Abstract: Combinations of perovskite-type oxides with transition and precious metals exhibit the remarkable self-regenerable property that could be exploited for numerous practical applications. The objective of the present work was to study the reversibility of structural changes of perovskite-type oxides under cyclic reducing/oxidizing atmosphere by taking advantage of the reducibility of $LaCoO_3$. $LaCoO_{3\pm\delta}$ and $LaCo_{0.8}Cu_{0.2}O_{3\pm\delta}$ were prepared by ultrasonic spray combustion and were characterized by scanning electron microscopy (SEM), X-ray diffraction (XRD), X-ray absorption spectroscopy (XAS) and temperature programmed reduction (TPR). XRD and XAS data confirmed that copper adopted the coordination environment of cobalt at the B-site of the rhombohedral $LaCoO_3$ under the selected synthesis conditions. The structural evolution under reducing atmosphere was studied by in situ XRD and XANES supporting the assignment of the observed structural changes to the reduction of the perovskite-type oxide from $ABB'O_3$ (B'=Cu) to B'^0/ABO_3 and to B'^0B^0/A_2O_3. Successive redox cycles allowed the observation of a nearly complete reversibility of the perovskite phase, i.e. copper was able to revert into $LaCoO_3$ upon oxidation. The reversible reduction/segregation of copper and incorporation at the B-site of the perovskite-type oxides could be used in chemical processes where the material can be functionalized by segregation of Cu and protected against irreversible structural changes upon re-oxidation.

Introduction

Perovskite-type oxides (ABO_3) are probably the most widely explored mixed-oxide systems in material science and especially in the field of heterogeneous catalysis.[1] The ideal perovskite structure is cubic, however it is rarely obtained at ambient temperature/pressure due to the strict constraints on the ionic sizes of A- and B-site cations and of oxygen. As a result, the distorted rhombohedral, the tetragonal and the orthorhombic monoclinic or triclinic symmetry are more diffused.[2] The design of complex perovskite-type oxides by tuning the nature of the A- and/or B-site cations has attracted broad scientific interest, because the resulting materials of general formula $A_{1-x}A'_xB_{1-y}B'_yO_{3\pm\delta}$ display a large variety of properties by accommodating cations of various sizes and valences.[3] For example, these mixed oxides can act as oxidation catalysts or as precursors for supported metal catalysts upon pre-treatment under reducing conditions that enables the controlled segregation of the B-site cation on a matrix of the A-site metal oxide (solid phase crystallization),[4] the B-site element representing the active phase. Such materials play an important role in catalytic processes like water gas shift, partial oxidation[5] and reforming of methane (dry and wet),[6] alkene hydrogenation,[7] alkane hydrogenolysis, higher alcohol synthesis,[8] and Fischer-Tropsch synthesis.[9] The in situ segregation strategy is also exploited for perovskite-type oxides central to solid oxide fuel cells (SOFC)[10] and for heterogeneous catalytic application for soot combustion[11] even some homogeneous application for selective hydrogenations.[12] Moreover, application of perovskite-type oxides in automotive exhaust catalysis has been demonstrated extensively.[13] The reversible segregation and reincorporation of platinum group metals (PGM; Pd, Rh, Pt) in various perovskite-type oxides[13c] was reported as a mean to produce well-dispersed catalytically active precious metal particles, to exploit their catalytic properties for demanding reactions including NO_x reduction and, finally to protect by reoxidation the PGM from particle sintering upon exposure to high temperature. Attempts to rationalize the mechanism of this self-regeneration concept and to provide guidance for further development were made by theory,[14] while electron microscopy was used to critically assess the extent and practical relevance of this property.[15] Recently, the segregation-dissolution approach was demonstrated for characteristic anode materials of SOFC with nickel as the active metal.[16] The boundary conditions necessary to achieve the self-regeneration of La-Fe-Ni-O mixed oxides claimed earlier[17] were defined using temperature programmed reduction, X-ray diffraction, X-ray absorption spectroscopy and electron microscopy.[18]

Cobalt exhibits the most reducible perovskite-type oxide among the simplest and most common $LaMnO_3$, $LaFeO_3$ and $LaCoO_3$ oxidation catalysts.[19] In automotive catalysis, this represents a drawback because of the danger of metallic Co to form and to leave the catalytic converter to the environment under severe reaction conditions.[20] The remarkable reducibility of $LaCoO_3$ was exploited especially to generate dispersed metal particles supported on the A-site metal oxide for other catalytic applications, as indicated above. There are only few observations in the literature reporting on the reversibility of the La-Co-O system under reducing treatments[21] and/or under operational conditions.[22] Kuc et al.[23] demonstrated that self-regeneration occurs in $LaCo_{1-x-y}Pd_xZn_yO_{3\pm\delta}$ upon reduction at 600 ºC and reoxidation at 800 ºC, while under the same conditions the homologous Fe-based perovskite is not able to regenerate the original structure, and used it to produce segregated Pd-Zn alloyed nanoparticles for methanol steam reforming.[24] The different behavior of the two perovskite-type oxides goes along with the observation that B-site occupancy by Pd strongly depends on perovskite-type composition (and structure)[19] and synthesis method.[25] Reoxidation of a La-Co-Ru-O catalyst at the low temperature of 500 ºC after reduction

[a] Dr. R. Pereñíguez
Instituto de Ciencia de Materiales de Sevilla and Dpto. Química Inorgánica. CSIC-Universidad de Sevilla
Av. Américo Vespucio, 49, E-41092 Sevilla (Spain)
E-mail: rosa@icmse.csic.es
[b] Dr. D. Ferri
Paul Scherrer Institut
CH-5232 Villigen PSI (Switzerland)

This document is the accepted manuscript version of the following article:
Pereñíguez, R., & Ferri, D. (2018). Structural reversibility of LaCo1-xCuxO3 followed by in situ X-ray diffraction and absorption spectroscopy. ChemPhysChem, 19(15), 1876-1885. https://doi.org/10.1002/cphc.201800069

under reaction conditions of preferential oxidation of CO (PROX) was likely not able to fully restore the initial structure but was sufficient to generate a more active catalyst.[26] Conversely, the activity of the same catalyst maintained under the reducing reaction conditions in heating/cooling segments without intermediate reoxidation decreased, demonstrating the beneficial aspects of reduction-reoxidation.

The aim of this work is to evaluate the structural reversibility of perovskite-type oxides based on $LaCoO_3$ through the segregation of the B^{3+} cation under reducing conditions and the subsequent recovery of the initial structure under oxidizing conditions. Cobalt substitution by copper is presented here,[27] because of the relevance and broad application range of this transition metal in various catalytic applications. Moreover, copper is a suitable candidate to study the structural reversibility in combination with $LaCoO_3$ because of the similar ionic size to cobalt. To the best of our knowledge, no evidence of the structural reversibility of a Co-Cu perovskite-type oxide ($LaCo_{1-x}Cu_xO_3$) exists in literature.

Results and Discussion

The SEM images of $LaCoO_3$ (LaCo) obtained by ultrasonic spray combustion (USC) at 600 ºC and after calcination at 600 ºC are shown in Figure 1a and Figure 1b, respectively. It is shown just the images of the system LaCo because the morphology of both samples (LaCo and LaCoCu) was identical; suggesting that addition of Cu did not modify the particle structure to a visible extent. The samples consisted of a heterogeneous size distribution of pseudo-spherical particles in the range of 0.05-3 µm. The particles possessed a hollow structure already after synthesis, which is an intrinsic consequence of the synthesis process.[28] USC implicates the evolution of a considerable amount of gaseous products inside the solid spherical particles originating from the precursor droplets produced by the ultrasonic nebulizer. After synthesis, the particle surface appeared compact and homogeneous (Fig. 1a). The morphology of the particle wall changed after calcination (Fig. 1b) and was composed of a single layer of nanoparticles of ca. 50 nm.

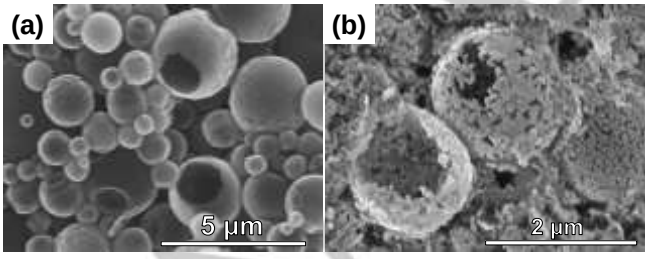

Figure 1. SEM micrographs of (a) synthesized and (b) calcined $LaCoO_3$.

The formation of these porous surfaces was completed during calcination, which was confirmed previously by the comparison of samples prepared by USC with and without citric acid.[28-29] Citric acid induces a similar process to that observed in the combustion synthesis[29-30] producing the characteristic morphology observed after calcination. The existence of well crystallized nanocrystals promoted by the low calcination temperature and the addition of citric acid,[29] which may inhibit the sintering process, is likely responsible for the porous spheres observed in Figure 1b. The BET specific surface area of the samples was significantly higher compared to the typical values (<10 m^2/g) reported for this type of materials prepared by conventional methods [31] and varied from 20.8 m^2/g of LaCo to 25.7 m^2/g of $LaCo_{0.8}Cu_{0.2}O_3$ (LaCoCu). The exploitation of citric acid appears to compensate the typical decrease in the specific surface area caused by the sintering process during calcination.

Figure 2a shows the X-ray diffraction (XRD) patterns of LaCo and LaCoCu after calcination at 600 ºC. Both samples exhibited the same rhombohedral perovskite structure of $LaCoO_3$ (ICDD, 01-084-0846, R-3c). The poorly resolved doublet of the rhombohedral crystal structure at ca. 32-34º (depending on the sample composition) revealed a low degree of crystallinity, which was likely a result of the low temperature employed for both the synthesis and the calcination. However, the selected temperature was sufficient to obtain the perovskite-like phase.

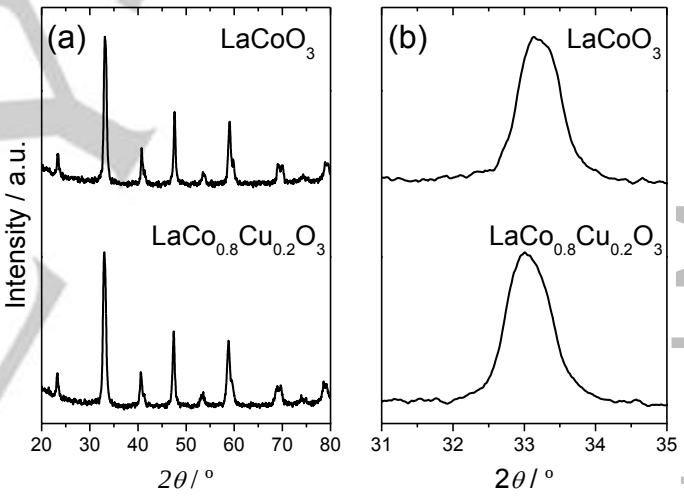

Figure 2. (a) XRD patterns of $LaCoO_3$ and $LaCo_{0.8}Cu_{0.2}O_3$. (b) Detail of the major reflection line.

Coordination state of Cu

The occupation of the B-site by copper was studied first by XRD. Figure 2b demonstrates that the major reflection of the rhombohedral structure of $LaCoO_3$ shifted to lower angles upon substitution of Co by 20% Cu. The shift can be associated with the insertion of copper in the cobalt position of the perovskite lattice (B-site) with the consequent distortion of the rhombohedral unit cell.[32] Despite the ambiguity of XRD with respect to the presence of low levels of other crystalline phases, the absence of diffraction lines attributed to other metal oxide phases (La, Co or Cu) supported the conclusion that all copper occupied the coordination position of cobalt in the $LaCoO_3$ perovskite lattice and confirmed the homogeneity of the LaCoCu perovskite phase.

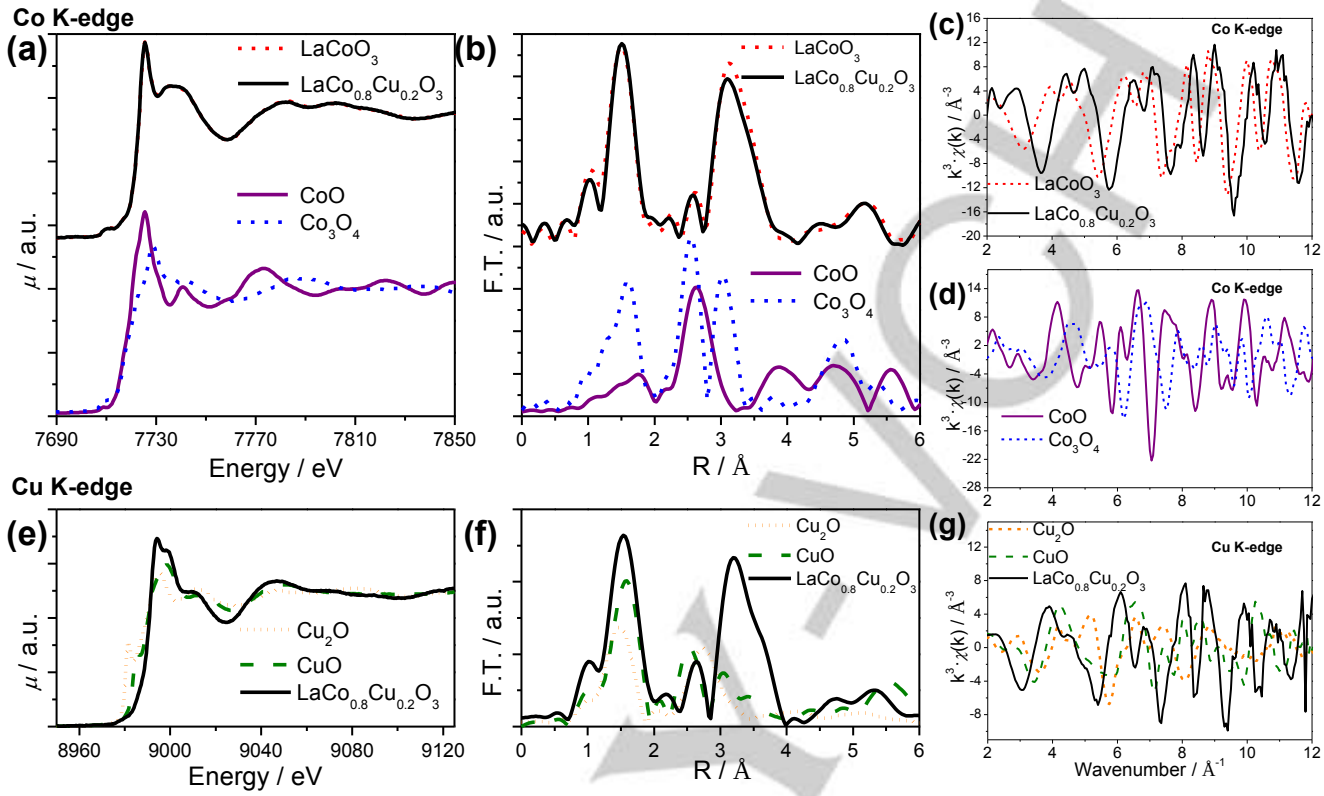

Figure 3. Co and Cu K-edges (a,e) XANES spectra, (b,f) non-phase corrected FT-EXAFS spectra and (c,d,g) k^3-weighted EXAFS oscillations of $LaCoO_3$ and $LaCo_{0.8}Cu_{0.2}O_3$. Reference compounds are also provided.

The coordination environment of the substituting metal can be better evaluated using a probe of local structure such as X-ray absorption spectroscopy (XAS). The X-ray absorption near edge (XANES) spectra (Figure 3a,e) and the Fourier transform (FT) of the extended X-ray absorption fine structure (EXAFS) region (Figure 3b,f) of the calcined samples were measured around the Co and Cu K-edges to obtain the local structure of cobalt and copper. The k^3-weighted EXAFS functions in the range 2-12 $Å^{-1}$ are included in Figure 3 (c,d,g). The Co K-edge XANES spectra of LaCo and LaCoCu (Figure 3a) were very similar to those obtained for cobaltites with perovskite-type structure.[33] Other phases can be discarded based on the values of the edge energy position (E_0), the whiteline and the post-edge oscillations, which were clearly different from those of the two reference cobalt oxides CoO and Co_3O_4 also shown in Figure 3a. The non-phase shifted FT spectrum of LaCo (Figure 3b) consisted of two main contributions at 1.5 and 3.1 Å, which are in agreement with those reported for the perovskite-type structure.[34] These represent the fingerprints of cobalt adopting the coordination environment of the B-site of $LaCoO_3$: the contribution at 1.5 Å corresponds to the first Co-O coordination shell, while the one at 3.1 Å invokes the Co-O-Co neighboors of the octahedral environment (Fig. 3b). The small intensity difference observed for the latter contribution in the presence of copper can be interpreted as being the result of some extent of structural disorder induced by introduction of the second metal at the B-site.[33a] The FT-spectra of CoO and Co_3O_4 did not coincide with respect to any feature to the spectrum of LaCo and LaCoCu. This is further supported by the spectra in k-range (Figure 3c,d). Based on these considerations and by comparison with the reported literature and the XRD data, the spectra of LaCo and LaCoCu at the Co K-edge revealed that Co was adopting the oxidation (+3) and octahedral coordination state of Co (CoO_6) in the perovskite-type structure.

The XANES (Figure 3e) and EXAFS (Figure 3f,g) spectra of LaCoCu obtained at the Cu K-edge were consistent with the reported spectra of Cu in $LaCuO_3$,[35] where Cu^{3+} occupies CuO_6 octahedra. The whiteline of the XANES region exhibited a typical doublet accompanied by a second post-edge feature at ca. 9010 eV. The XANES spectrum was very different from those of the reference oxides CuO and Cu_2O and evidenced no pre-edge features, thus allowing us to associate the XANES region to copper species in oxidation state higher than +2. Two main coordination spheres were observed in the FT spectrum (Figure 3f) at 1.5 Å (Cu-O) and 3.2 Å (Cu-O-Cu) that resembled closely those observed for cobalt in the perovskite structure (Figure 3b). Also in this case, comparison with the EXAFS spectra (FT and k-range) of the reference oxides clearly confirmed that Cu adopting the coordination environment of other phases (such as CuO and Cu_2O) can be discarded. Therefore, Cu (likely Cu^{3+})

was in the coordination environment and oxidation state of the B-site of $LaCoO_3$.

The XRD patterns and the EXAFS/XANES spectra of LaCoCu demonstrated that under these synthesis conditions and at this substitution level, Cu was homogeneously distributed in the $LaCoO_3$ structure and occupied the B-site.[36]

Reducibility

After assessing the formation of LaCoCu with homogeneous distribution of copper at the B-site within the perovskite-type oxide, the reducibility of this structure is a key point in order to design a functional material based on the concept of the reversible segregation-dissolution of a metal, which is relevant for example for catalytic processes. Therefore, the reducibility of the perovskite-like samples was investigated using H_2 temperature programmed reduction (TPR-1, 5 vol% H_2/Ar, Figure 4) and consecutive reduction-oxidation cycles (repeated 5 vol% H_2/Ar and 3 vol% O_2/He, Figure 4). The structural evolution during TPR was complemented by in situ XRD on a lab scale instrument under 5 vol% H_2/N_2, and the diffractograms recorded for each experiment are presented in Figure 5 (TPR-1) and Figure 6 (TPR-2). It should be noted that the evolution of the crystalline phases may not exactly match the TPR profiles of Figure 4 because of the differences in the operation mode of each experiments. Figure 4a and Figure 4b show the profiles of hydrogen consumption during the TPR measurements on calcined LaCo and LaCoCu, respectively. The reduction profiles presented two well separated peaks at 200-400 ºC and 450-650 ºC, which were assigned to two distinct reduction events. The reduction of both samples was completed before 650 ºC. A slight shift of 30-50 ºC to lower temperatures was detected for both samples just after the first TPR, remaining the shape of the profiles for TPR-2 and TPR-3. This effect was also previously reported for other perovskite composition,[37] then we ascribed this difference to a soft structural reordering in perovskites, due to the higher temperature applied in comparison with the one used for calcination, that does not affect to the phases composition (not evidences of new phases by the rest of the characterization) but may make the material slightly more reducible.

Decomposition of the TPR-1 peaks shown in Figure 4 provides a quantitative measure of the steps involved in the reduction process (Table 1). The variation of the oxidation state of the active metal was expressed using the theoretical (Δn_T^+) and the experimental (Δn_E^+) consumption of H_2 required to completely reduce the perovskite-type oxide ($LaBO_3$) to B^0 and La_2O_3.[26] Δn_T^+ was estimated taking into account the oxidation state inferred from the XAS data discussed in Figure 3 (Co^{3+} in LaCo). The quantitative data for LaCo allowed us to ascribe the two peaks shown in the TPR profile of Figure 4a to the following reduction steps. The first event at low temperature (375 and 400 ºC) was associated with the $Co^{3+}\rightarrow Co^{2+}$ reduction (Table 1).[31d, 38] Previous in situ XAS studies confirmed this assignment.[33a, 39] This reduction step is characterized by the loss of oxygen from $LaCoO_3$ to produce the intermediate brownmillerite-like phases, $La_3Co_3O_8$ and $La_2Co_2O_5$.[39] The reduction of the cobaltite ended after the high temperature reduction peak at 570 ºC, where the perovskite phase based on divalent cobalt completely vanished in favor of metallic cobalt and La_2O_3 ($Co^{2+}\rightarrow Co^0$). The Δn_E^+ calculated for both processes was very similar to the theoretical one, thus substantiating this mechanism. This evaluation neglected the presence of two brownmillerite phases and considered only the formal change from oxidation state +3 to +2.

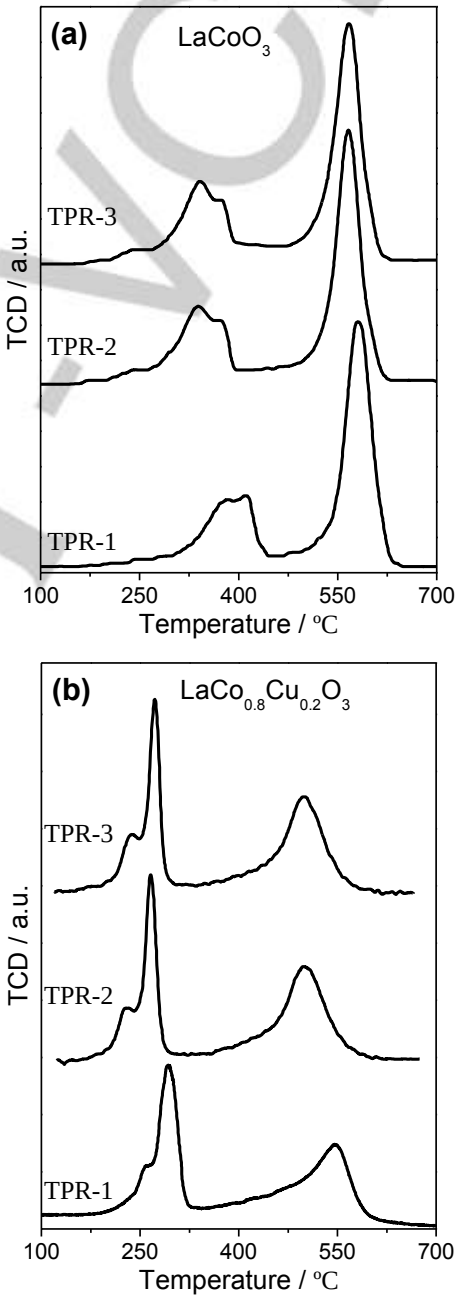

Figure 4. Consecutive H_2-TPR profiles of (a) $LaCoO_3$ and (b) $LaCo_{0.8}Cu_{0.2}O_3$. The TPR were alternated by a temperature programmed oxidation as detailed in the main text.

The in situ XRD patterns of LaCo during TPR-1 in Figure 5a show that the rhombohedral structure survived the reducing treatment until ca. 450 ºC. The increase of temperature caused initially only a shift of the diffraction lines to lower diffraction angles (higher d-spacing) in both samples as a result of thermal expansion. Between 450 and 500 ºC the XRD pattern changed to that of $La_2Co_2O_5$, in agreement with the partial reduction of $LaCoO_3$ ($Co^{3+}\rightarrow Co^{2+}$) observed in TPR-1 (Figure 4a). Contrary to observations on $LaCo_{0.95}Pd_{0.05}O_3$,[39] there was no explicit indication of an intermediate step producing $La_3Co_3O_8$ except for a multiple reflection at 32.5º and 33º in a narrow temperature range (450-500 ºC) that may justify the sharp peak observed in TPR-1 at 400 ºC and could reflect the $La_3Co_3O_8\rightarrow La_2Co_2O_5$ transition. Once formed, the $La_2Co_2O_5$ brownmillerite was visible until the end of the measurement. Finally, at 700 ºC, the XRD pattern exhibited initial contributions of hexagonal La_2O_3 (refection at ca. 30º). The appearance of La_2O_3 was an evidence of the destruction of the perovskite-like phase and the reduction of cobalt to Co^0 ($La_2Co_2O_5 + 2H_2 \rightarrow 2Co + La_2O_3 + 2H_2O$), whose presence was difficult to appreciate in the diffractograms.

Table 1. Reduction steps, temperatures of H_2 consumption (T_m), theoretical (Δn_T^+) and experimental (Δn_E^+) extent of electron exchange obtained from the TPR profiles of $LaCoO_3$ and $LaCo_{0.8}Cu_{0.2}O_3$.

Entry	Step	T_m (ºC)	Δn_T^+	Δn_E^+
$LaCoO_3$	$Co^{3+}\rightarrow Co^{2+}$	375	1	1.1
		400		
	$Co^{2+}\rightarrow Co^0$	570	2	1.9
$LaCo_{0.8}Cu_{0.2}O_3$	$Cu^{3+}\rightarrow Cu^{(3-x)+}$	250	$(x)0.2^{Cu}$	0.23
	$Cu^{(3-x)+}\rightarrow Cu^0$	285	$(3-x)0.2^{Cu}+0.8^{Co}$	1.1
	$Co^{3+}\rightarrow Co^{2+}$	285		
	$Co^{2+}\rightarrow Co^0$	475	1.6	1.67
		540		

The introduction of copper in the lattice of $LaCoO_3$ changed significantly the reduction process (Figure 4b), which was completed at around 625 ºC, but did not modify the extent of H_2 consumption (Table 2). The reduction events observed for LaCo shifted to 285 and 540 ºC indicating that copper facilitated reduction of the cobaltite[31a, 31b, 32b, 38a, 40] and the low temperature event intensified at the expenses of the high temperature one.

XAS data indicated that cobalt and copper were present as Co^{3+} and Cu^{3+} in LaCoCu suggesting that the quantification of the reduction processes should start from these oxidation states. Based on the quantitative data collected in Table 1 together with the in situ XRD data, the additional component at 250 ºC was tentatively assigned to the partial reduction of copper, i.e. $Cu^{3+}\rightarrow Cu^{(3-x)+}$. The second large reduction event centered at 285 ºC was ascribed to the complete reduction of copper to Cu^0 accompanied by the first step of cobalt reduction, $Co^{3+}\rightarrow Co^{2+}$.[31b]

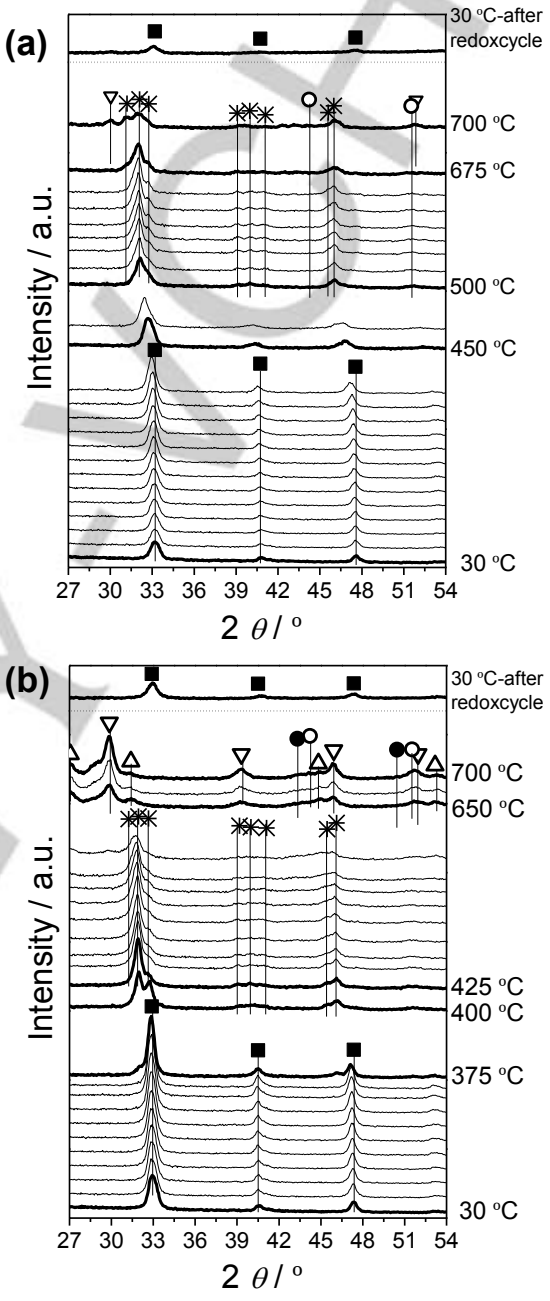

Figure 5. In situ XRD patterns of (a) $LaCoO_3$ and (b) $LaCo_{0.8}Cu_{0.2}O_3$ recorded during H_2-TPR-1 and the reoxidized one after this H_2-TPR-1. Crystalline phases: ■-$LaCoO_3$-Rombohedral; ✳-$La_2Co_2O_5$+$La_3Co_3O_8$-Brownmillerite; ◆-La_2CoO_4-Tetragonal; O-Co-cubic; ●-Cu-cubic; ▽-La_2O_3-Hexagonal; △-La_2O_3-Cubic.

The decrease in the temperature of the latter process (lower by ca. 100 ºC) compared with the value obtained for LaCo was associated with the electronic interaction between copper and

cobalt in the perovskite lattice.[40-41] As reduction of copper proceeded, hydrogen dissociation on Cu^0 and subsequent spill-over to the vicinal cobalt ions promoted reduction of $LaCoO_3$.[42] Similar to LaCo, the high temperature peak mirrored the complete reduction of the perovskite structure ($Co^{2+}\rightarrow Co^0$). Given the lower extent of temperature shift (only 30 ºC) compared to the $Co^{3+}\rightarrow Co^{2+}$ reduction, this event seemed less sensitive to the presence of copper and is probably related to a lower interaction between the Cu^0 entities and Co^{2+}.

Figure 5b confirms that the structural changes in the B-site substituted cobaltite occurred at different temperatures. The first step associated with the formation of the brownmillerite phase was anticipated by ca. 100 ºC and started to appear at 375 ºC in LaCoCu. Hexagonal and cubic La_2O_3 appeared at 650 ºC and reduction of LaCoCu was completed before 700 ºC. This substantiated the role of Cu in promoting the total reduction process of $LaCoO_3$ that was around 50 ºC lower. According to the thermogram of LaCoCu and the in situ XRD data, we conclude that the metallic Cu particles segregate on a brownmillerite-type sample starting at ca. 350 ºC. This Cu^0 phase is less accessible to the interaction with the remaining Co^{2+}-containing phase than homogeneously dispersed copper ions. Hence, copper modifies the second reduction process, i.e. $Co^{2+}\rightarrow Co^0$ to a lesser extent.

Table 2. Theoretical (TPR_T) and experimental (TPR-1 to TPR-3) H_2 consumption (mmol) of $LaCoO_3$ and $LaCo_{0.8}Cu_{0.2}O_3$ in the consecutive TPR measurements.

Entry[a]	TPR_T	TPR-1[b]	TPR-2[c]	TPR-3
$LaCoO_3$	80	81	84	83
$LaCo_{0.8}Cu_{0.2}O_3$	77	78	74	75

Structural reversibility

Once the homogeneity of coordination of the B-site elements upon variation of sample composition was ascertained and the behavior of the samples under reducing conditions was established, some effort was undertaken to explore the reversibility of these structural changes. For this purpose, TPR was used in three consecutive reduction-oxidation cycles (TPR-TPO) as shown in Figure 4. Each heating-cooling TPR measurement was followed by a heating-cooling TPO measurement. Two general aspects are evident for both samples: i) the first TPR profile (discussed above) was slightly different from the second and third TPR in terms of reduction temperatures, while ii) the thermograms were very similar after the first redox cycle (TPR followed by oxidation at 700 ºC). Table 2 demonstrates that the H_2 consumption calculated from the total area of each TPR measurement was very similar suggesting that the extent of reduction (H_2 consumption) was identical between the three TPR runs.

Figure 5a-top and Figure 5b-top show the XRD patterns of the samples after a redox cycle (TPR and oxidation in air in a heating segment from 30 to 700 ºC, i.e. before TPR-2). It is clear that after oxidation at 700 ºC for 10 min the initial rhombohedral phase was recovered and no evidence of any other crystalline phase was provided by XRD. Hence, the second cycle (TPR-2) started from a very similar phase composition compared with the calcined samples.

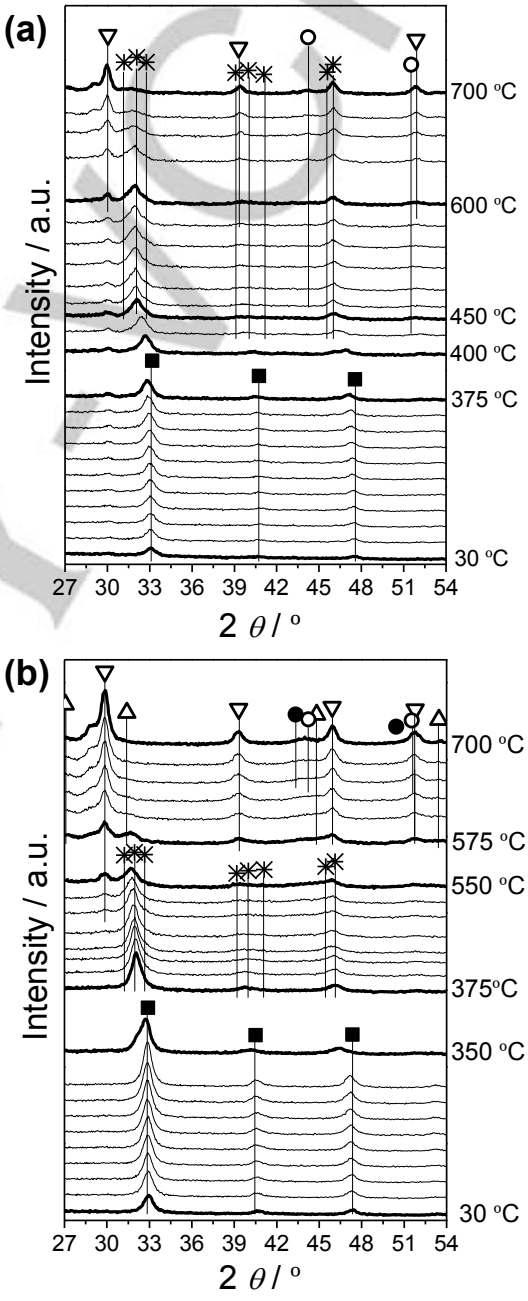

Figure 6. In situ XRD patterns of (a) $LaCoO_3$ and (b) $LaCo_{0.8}Cu_{0.2}O_3$ recorded during H_2-TPR-2. Crystalline phases: ■-$LaCoO_3$-Rombohedral; ✳-$La_2Co_2O_5$+$La_3Co_3O_8$-Brownmillerite; ◆-La_2CoO_4-Tetragonal; ○-Co-cubic; ●-Cu-cubic; ▽-La_2O_3-Hexagonal; △-La_2O_3-Cubic.

In the second reduction (5 vol% H_2/Ar, 30-700 ºC; XRD Figure 6) after oxidation in air (from 30 to 700 ºC), the overall structural evolution observed in TPR-1 shifted by ca. 25-50 ºC to lower temperature. This behaviour agrees qualitatively with the differences observed in the consecutive TPR measurements of Figure 4. Based on these observations, we consider that in these samples the perovskite phase is highly reversible through redox cycles. However, it changes its redox and structural properties partially.

Next, we focused our attention on the more complex system, LaCoCu, and studied the response of its structure to redox cycles using in situ XAS and synchrotron XRD. The experimental protocol presented in Scheme 1 consisted in the following segments: equilibration in He at room temperature (RT, XRD and XANES recorded in position 1); reduction from room temperature to 625 ºC in 5 vol% H_2/Ar (Reduction-1, pos. 2); oxidation in 20 vol% O_2/He at 625 ºC for 30 min (Oxidation-1, pos. 3); reduction at 625 ºC in 5% vol% H_2/Ar for 30 min (Reduction-2, pos. 4); oxidation in 20 vol% O_2/He at 625 ºC for 30 min (Oxidation-2, pos. 5) and equilibration in He at room temperature (end, pos. 6). The XANES spectra recorded around the Co K-edge and the Cu K-edge are reported in Figure 7a and Figure 7b, respectively. The quasi-simultaneous XRD patterns recorded during the temperature programmed reduction are shown in Figure 7c. Finally, Figure 7d summarizes the XRD patterns obtained at the end of the different positions described in Scheme 1.

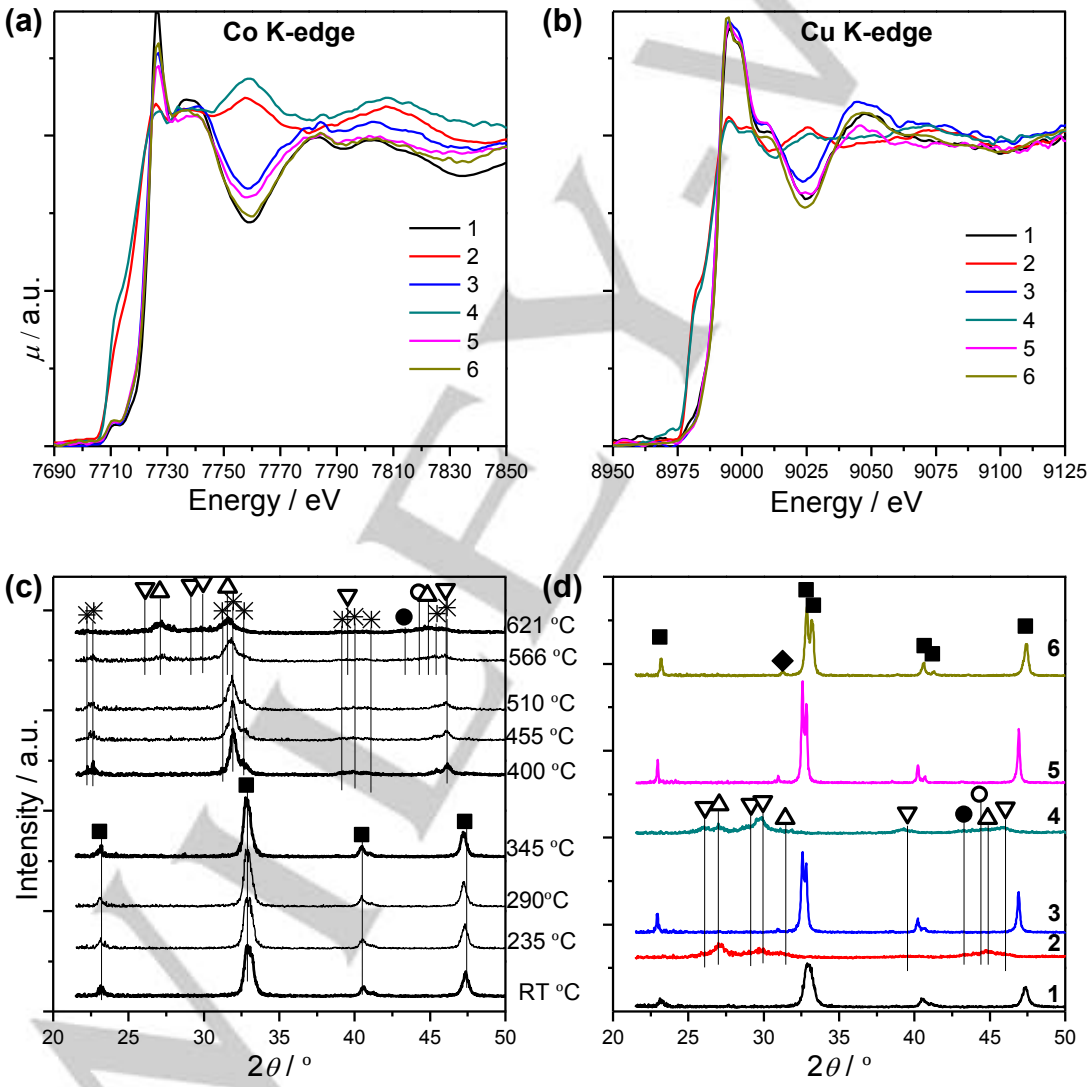

Figure 7. (a) Co K-edge, (b) Cu K-edge in situ XANES spectra and (d) In situ XRD patterns of $LaCo_{0.8}Cu_{0.2}O_3$ under varying atmosphere identified in Scheme 1. (c) In situ XRD patterns obtained during the initial TPR measurement. Crystalline phases: ■-$LaCoO_3$-Rombohedral; ✳-$La_2Co_2O_5$+$La_3Co_3O_8$-Brownmillerite; ◆-La_2CoO_4-Tetragonal; ○-Co-cubic; ●-Cu-cubic; ▽-La_2O_3-Hexagonal; △-La_2O_3-Cubic.

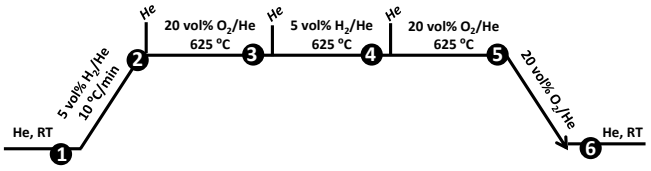

Scheme 1. Experimental protocol of the in situ studies.

The Co and Cu K-edge XANES spectra of LaCoCu recorded at room temperature exhibited the same characteristics discussed in Figure 3. After TPR, the Co K-edge spectrum recorded at 625 ºC in reducing atmosphere clearly showed a loss of whiteline intensity, a shift of E_0 to lower energy values and a different distribution in the post-edge oscillations. All these changes point to the reduction of Co^{3+} to Co^0. The XANES spectrum around the Cu K-edge also suggests that copper was reduced significantly at this temperature. The corresponding XRD pattern of LaCoCu under these conditions (Figure 7c) demonstrates that the perovskite structure was almost completely lost upon TPR and hexagonal and cubic La_2O_3 was formed after formation of the intermediate brownmillerite phase from 400 ºC in agreement with the previous data shown in Figures 4 and 5. Hence, XRD and XAS show that the sample was almost completely reduced to Cu^0+Co^0/La_2O_3 at 625 ºC. However, comparison of the XRD data recorded in positions 2 and 4 (Figure 7d) showing the remaining reflections of the brownmillerite phase at 621 ºC reveals that the reduction was not complete at the end of the TPR (Figure 7c, 621 ºC). This can be explained considering that the exposure time under reducing atmosphere in these measurements (pos. 2 and pos. 4) was longer compared to the TPR runs. The reflections of hexagonal La_2O_3 were more pronounced after the second reduction (pos. 4) than after TPR-1 (pos. 2), confirming that the reduction of the perovskite-like phase was completed after the second reduction.

The XRD patterns confirmed that the perovskite phase was always recovered after both reoxidation segments at 625 ºC (pos. 3 and pos. 5). The small peak appearing at 31º indicates the formation of the tetragonal La_2CoO_4 spinel phase that cannot be easily verified by XANES. In the XANES spectra, the oxidation of cobalt into the perovskite-type structure was manifested by the restoration of all features of Co in the original $LaCoO_3$ structure. Similarly, the spectra at the Cu K-edge showed that Cu adopted the same structure as in the starting sample in both oxidation segments. Finally, the XANES spectra of LaCo and LaCoCu recorded at room temperature after cooling in oxygen (pos. 6) were identical to those measured before TPR (pos. 1). Therefore, both cobalt and copper experienced segregation upon reduction at 625 ºC and were able to regress into the perovskite-like structure upon exposure to oxygen at the same temperature.

This experiment demonstrates the reversibility of the structural changes of LaCoCu upon redox cycles based on considerations of the crystalline phases (XRD), the cobalt (XANES Co K-edge) and the copper (XANES Cu K-edge) oxidation states.

Conclusions

The selected synthesis method and conditions allowed the preparation of $LaCoO_3$ and Cu-substituted $LaCoO_3$ perovskites with rhombohedral structure. XRD and XAS data confirm the insertion of copper in the B site of the perovskite and that cupper adopts the coordination environment of cobalt. This composition change by copper modifies the reducing properties of the cobaltite resulting in an easier material to reduce. In situ XRD and XANES data during reduction and oxidation of the perovskite-type oxides demonstrated that copper reduced to metal under reducing conditions and reverted into the B-site of $LaCoO_3$ upon oxidation at 500 ºC thus generating a similar material to the starting one. In principle, this reversible reduction-oxidation could be exploited to design materials where generation of metallic copper imparts a specific functionality that can be protected upon oxidation and restored upon reduction. Alternately, this functionality could be exploited in cyclic redox conditions. The exact extent of such property needs to be characterized by further advanced probes of local structure for it to be called self-regeneration as we see that under the conditions proposed here it is not complete. In that sense, a possible catalytic reaction with a reductive atmosphere could be Preferential Oxidation of CO following by an oxidative treatment to explore its regeneration, then we will test these systems in order to evaluate its self-regeneration under this catalytic application.

Experimental Section

Synthesis of materials

The perovskite-type materials were synthesized by ultrasonic spray combustion (USC)[29, 43] using the experimental equipment described in detail elsewhere.[28] Briefly, a precursor solution was atomized using an ultrasonic nebulizer composed of three piezoelectric oscillators. The generated microdroplets were transported by a flow of 1 L/min air through a vertical quartz glass reactor installed in a furnace set at the desired synthesis temperature. The formation of the oxide phase takes place while the precursor solution droplets travel through the furnace. The resulting oxide powder was collected and dried on a membrane filter (mixed cellulose ester, 0.45 µm; Whatman) installed in a quartz glass pipe heated at 150 ºC to avoid physical blocking. A vacuum pump ensured continuous flow through the filter. The production rate was ca. 150-200 mg/h.

The aqueous precursor solution contained the metal salts ($La(NO_3)_3{\cdot}6H_2O$, Fluka, >99%; $Co(NO_3)_2{\cdot}6H_2O$, Sigma–Aldrich, >98%;

$Cu(NO_3)_2 \cdot 3H_2O$, Fluka, 99-104%) and citric acid (Riedel-de Haën, >99.5%) in the necessary molar ratio to obtain $LaCoO_{3-\delta}$ (LaCo) and $LaCo_{0.8}Cu_{0.2}O_{3-\delta}$ (LaCoCu). The ratio between the amount of citric acid and the total amount of metal ions was fixed at one. During synthesis, the oven temperature was set at 600 ºC, while all samples were calcined in air at 600 ºC for 4 h after collection onto the filter.

Characterization

X-ray diffractograms (XRD) of the synthesized and calcined powders were recorded with a Philips X'pert Pro MPD diffractometer in the Bragg-Brentano configuration and using Ni-filtered Cu Kα radiation (λ= 1.5418 Å). Patterns were collected in the 2θ range 20-80º with a step of 0.017º and an acquisition time of 1 s/point. For the in situ experiments under reducing conditions, the diffractograms were recorded with a Philips X´Pert pro diffractometer using the above configuration but in the 2θ range 24-56º with a step of 0.05º. The reduction of the perovskite-type structure was studied in flowing 5 vol% H_2/Ar from room temperature to 700 ºC at a rate of 10 ºC/min while recording diffractograms at steady state after every increment of 25 ºC.

Scanning electron microscopy (SEM) images were obtained with a field emission filament at an accelerating voltage of 5-10 kV and an extraction current of 10 µA on a Hitachi S-4800 microscope.

The specific surface area was measured with a Micromeritics ASAP 2020 instrument from N_2 adsorption-desorption isotherms at -196 ºC using the BET method. Prior to the measurement, the sample was degassed at 350 ºC for 2 h.

Temperature programmed reduction (H_2-TPR) experiments were performed according to the work of Malet and Caballero.[44] The setup is equipped with a thermal conductivity detector (TCD) previously calibrated using CuO and a mass spectrometer (MS) in line with the TCD used to quantify the H_2 concentration. To assess the degree of structural reversibility, three successive cycles of reduction (H_2-TPR) and oxidation were performed. After the first H_2-TPR in 5 vol% H_2/Ar (50 mL/min) from room temperature to 700 ºC at 10 ºC/min (TPR-1), the sample was cooled to room temperature in H_2/Ar. After purging with He, temperature programmed oxidation (TPO) was recorded in 3 vol% O_2/He (25 mL/min) in the same temperature range and at the same heating rate. Three consecutive TPR-TPO cycles were recorded using this methodology (TPR-2 and TPR-3).[26]

Quasi-simultaneous X-ray absorption spectra and XRD data were collected at the Swiss Norwegian beamline (SNBL) of the ESRF (Grenoble, France) under reducing and oxidizing conditions. For this purpose, the sample (ca. 1.5 mg) was firmly fixed between two quartz wool plugs in a quartz glass capillary cell (d= 1.5 mm). The setup was completed by a gas blower to control the capillary temperature and a manifold to introduce the desired gas mixture. A 0.5 mm thermocouple was inserted at the beginning of the sample bed to continuously monitor the sample temperature. The gas phase was measured using a MS (Omnistar, Pfeiffer) installed at the exit of the capillary reactor. H_2-TPR (5 vol% H_2/He) runs were performed up to 625 ºC at a heating rate of 5 ºC/min. The reversibility of the crystal phase and of the oxidation state changes was controlled by re-oxidizing the sample in air (20 vol% O_2/He) after reduction at 625 ºC.

XAS spectra (XANES and EXAFS) were collected in transmission mode at the Co (7709 eV) and Cu (8979 eV) K-edges at a variable energy step and 0.5 eV step across the XANES region. During the heating ramp, XANES spectra of 1 min were collected to avoid significant difference in temperature between the spectra. Spectra of oxidized phases of Co and Cu were recorded using standard reference samples. For energy calibration, Co or Cu foils were inserted after the second ionization chamber and measured simultaneously to the sample. EXAFS spectra were analysed using the analysis package ATHENA.[45] In situ time-resolved XRD data were measured with a high resolution diffractometer (λ = 0.50496 Å) and a six-channel detector. Data were collected in the range of 2θ= 21-107º resulting in the acquisition time of 97 s/pattern. XAS and XRD data were collected continuously and alternately at room temperature and during the temperature ramp.

Acknowledgements

The authors kindly acknowledge the financial support from the Spanish Ministry of Research (Project CTQ2014-60524-R), the IV Plan Propio of the University of Seville for a scholarship for R.P. and the Swiss National Science Foundation (SNF). The European Synchrotron Research Facility (ESRF) is acknowledged for beamtime allocation at the Swiss-Norwegian beamline (SNBL). The assistance of Dr. A. Kambolis and A. Rodriguez-Gomez during beamtime is highly appreciated. Part of this work was performed at the Swiss Federal Laboratories for Materials Science and Technology (Empa).

Keywords: $LaCoO_3$ • copper • in situ XRD • in situ XAS • structure reversibility

[1] S. Royer, D. Duprez, F. Can, X. Courtois, C. Batiot-Dupeyrat, S. Laassiri, H. Alamdari, *Chem. Rev.* **2014**, *114*, 10292.

[2] a) M. A. Pena, J. L. G. Fierro, *Chemical Reviews* **2001**, *101*, 1981-2017; b) R. J. H. Voorhoeve, D. W. Johnson, J. P. Remeika, P. K. Gallagher, *Science* **1977**, *195*, 827-833.

[3] H. Tanaka, M. Misono, *Current Opinion in Solid State & Materials Science* **2001**, *5*, 381-387.

[4] K. Takehira, *Catalysis Surveys from Japan* **2002**, *6*, 19-32.

[5] R. Lago, G. Bini, M. A. Pena, J. L. G. Fierro, *Journal of Catalysis* **1997**, *167*, 198-209.

[6] J. Guo, H. Lou, Y. Zhu, X. Zheng, *Materials Letters* **2003**, *57*, 4450-4455.

[7] J. O. Petunchi, M. A. Ulla, J. A. Marcos, E. A. Lombardo, *Journal of Catalysis* **1981**, *70*, 356-363.

[8] a) J. A. Brown Bourzutschky, N. Homs, A. T. Bell, *Journal of Catalysis* **1990**, *124*, 52-72; b) P. R. Watson, G. A. Somorjai, *Journal of Catalysis* **1982**, *74*, 282-295.

[9] L. Bedel, A. C. Roger, C. Estournes, A. Kiennemann, *Catalysis Today* **2003**, *85*, 207-218.

[10] a) D. Neagu, G. Tsekouras, D. N. Miller, H. Menard, J. T. S. Irvine, *Nature Chem.* **2013**, *5*, 916; b) Y.-F. Sun, Y.-Q. Zhang, J. Chen, J.-H. Li, Y.-T. Zhu, Y.-M. Zeng, B. S. Amirkhiz, J. Li, B. Hua, J.-L. Luo, *Nano Letters* **2016**, *16*, 5303-5309; c) L. Ye, M. Zhang, P. Huang, G. Guo, M. Hong, C. Li, J. T. S. Irvine, K. Xie, *Nature Communications* **2017**, *8*.

[11] Y.-F. Sun, J.-H. Li, Y.-Q. Zhang, B. Hua, J.-L. Luo, *ACS Catal.* **2016**, *6*, 2710-2714.

[12] X. Gong, M. Wang, H. Fang, X. Qian, L. Ye, X. Duan, Y. Yuan, *Chemical Communications* **2017**, *53*, 6933-6936.

[13] a) D. Fino, S. Bensaid, M. Piumetti, N. Russo, *Appl. Catal. A-Gen.* **2016**, *509*, 75-96; b) S. Keav, S. K. Matam, D. Ferri, A. Weidenkaff, *Catalysts* **2014**, *4*, 226-255; c) Y. Nishihata, J. Mizuki, T. Akao, H. Tanaka, M. Uenishi, M. Kimura, T. Okamoto, N. Hamada, *Nature* **2002**, *418*, 164; d) C. H. Kim, G. Qi, K. Dahlberg, W. Li, *Science* **2010**, *327*, 1624.

[14] a) H. Kizaki, K. Kusakabe, S. Nogami, H. Katayama-Yoshida, *Appl. Phys. Express* **2008**, *1*, 104001; b) S. Yanagisawa, A. Uozumi, I. Hamada, Y. Morikawa, *J. Phys. Chem. C* **2013**, *117*, 1278; c) I. Jarrige, K. Ishii, D. Matsumura, Y. Nishihata, M. Yoshida, H. Kishi, M. Taniguchi, M. Uenishi, H. Tanaka, H. Kasai, J. Mizuki, *ACS Catal.* **2015**, *5*, 1112.

[15] a) M. B. Katz, S. Zhang, Y. Duan, H. Wang, M. Fang, K. Zhang, B. Li, G. W. Graham, X. Pan, *J. Catal.* **2012**, *293*, 145; b) S. Dai, S. Zhang, M. B. Katz, G. W. Graham, X. Pan, *ACS Catal.* **2017**, *7*, 1579.

[16] D. Burnat, R. Kontic, L. Holzer, P. Steiger, D. Ferri, A. Heel, *J. Mater. Chem. A* **2016**, *4*, 11939.

[17] J. Deng, M. Cai, W. Sun, X. Liao, W. Chu, X. S. Zhao, *ChemSusChem* **2013**, *6*, 2061.

[18] P. Steiger, R. Delmelle, D. Foppiano, L. Holzer, A. Heel, M. Nachtegaal, O. Kröcher, D. Ferri, *ChemSusChem* **2017**, *10*, 2505.

[19] A. Eyssler, A. Winkler, O. Safonova, M. Nachtegaal, S. K. Matam, P. Hug, A. Weidenkaff, D. Ferri, *Chem. Mater.* **2012**, *24*, 1864.

[20] I. Tan, H. Tanaka, M. Uenishi, K. Kaneko, S. Mitachi, *J. Ceram. Soc. Jpn.* **2005**, *113*, 71.

[21] Z. Y. Zhao, L. Wang, J. Ma, Y. F. Feng, X. M. Cao, W. C. Zhan, Y. L. Guo, Y. Guo, G. Z. Lu, *RSC Adv.* **2017**, *7*, 15211-15221.

[22] Y. Nishihata, J. Mizuki, T. Akao, H. Tanaka, M. Uenishi, M. Kimura, T. Okamoto, N. Hamada, *Nature* **2002**, *418*, 164-167.

[23] J. Kuc, Y. Zhang, R. Erni, S. Yoon, L. Karvonen, A. Weidenkaff, S. K. Matam, *Phys. Status Solidi RRL* **2015**, *9*, 282.

[24] J. Kuc, M. Neumann, M. Armbrüster, S. Yoon, Y. Zhang, R. Erni, A. Weidenkaff, S. K. Matam, *Catal. Sci. Technol.* **2016**, *6*, 1455.

[25] Y. Lu, A. Eyssler, E. H. Otal, S. K. Matam, O. Brunko, A. Weidenkaff, D. Ferri, *Catal. Today* **2013**, *208*, 42.

[26] R. Pereniguez, A. Caballero, D. Ferri, *Catal. Commun.* **2017**, *92*, 75.

[27] a) G. Avgouropoulos, T. Ioannides, H. Matralis, J. Batista, S. Hocevar, *Catalysis Letters* **2001**, *73*, 33-40; b) T. Caputo, R. Pirone, G. Russo, *Kinet Catal* **2006**, *47*, 756-764.

[28] X. Wei, P. Hug, R. Figi, M. Trottmann, A. Weidenkaff, D. Ferri, *Appl. Catal. B:Environmental* **2010**, *94*, 27-37.

[29] R. Pereniguez, V. M. Gonzalez-delaCruz, A. Caballero, J. P. Holgado, *Appl. Catal. B:Environmental* **2012**, *123*, 324-332.

[30] V. M. Gonzalez-Delacruz, F. Ternero, R. Pereniguez, A. Caballero, J. P. Holgado, *Appl. Catal. A:General* **2010**, *384*, 1-9.

[31] a) F. S. Toniolo, R. N. S. H. Magalhães, C. A. C. Perez, M. Schmal, *Appl. Catal. B:Environmental* **2012**, *117-118*, 156-166; b) N. Tien-Thao, H. Alamdari, S. Kaliaguine, *J. Solid State Chem.* **2008**, *181*, 2006-2019; c) A. A. A. daSilva, M. C. Ribeiro, D. C. Cronauer, A. J. Kropf, C. L. Marshall, P. Gao, G. Jacobs, B. H. Davis, F. B. Noronha, L. V. Mattos, *Top. Catal.* **2014**, *57*, 637-655; d) R. Pereniguez, J. L. Hueso, J. P. Holgado, F. Gaillard, A. Caballero, *Catal. Lett.* **2009**, *131*, 164-169.

[32] a) P. Porta, S. DeRossi, M. Faticanti, G. Minelli, I. Pettiti, L. Lisi, M. Turco, *J. Solid State Chem.* **1999**, *146*, 291-304; b) R. Zhang, A. Villanueva, H. Alamdari, S. Kaliaguine, *Appl. Catal. B:Environmental* **2006**, *64*, 220-233.

[33] a) J. L. Hueso, J. P. Holgado, R. Pereniguez, S. Mun, M. Salmeron, A. Caballero, *J. Solid State Chem.* **2010**, *183*, 27-32; b) O. Toulemonde, N. N'Guyen, F. Studer, A. Traverse, *J. Solid State Chem.* **2001**, *158*, 208-217.

[34] O. Haas, C. Ludwig, U. Bergmann, R. N. Singh, A. Braun, T. Graule, *J. Solid State Chem.* **2011**, *184*, 3163-3171.

[35] a) J. H. Choy, D. K. Kim, S. H. Hwang, G. Demazeau, *Phys. Rev. B* **1994**, *50*, 16631-16639; b) A. W. Webb, K. H. Kim, C. Bouldin, *Solid State Commun.* **1991**, *79*, 507-508.

[36] C. Weigl, K.-J. Range, *Journal of Alloys and Compounds* **1993**, *200*, L1-L2.

[37] R. Pereniguez, V. M. Gonzalez-DelaCruz, J. P. Holgado, A. Caballero, *Applied Catalysis B-Environmental* **2010**, *93*, 346-353.

[38] a) L. Huang, M. Bassir, S. Kaliaguine, *App. Surf. Sci.* **2005**, *243*, 360-375; b) N. A. Merino, B. P. Barbero, P. Grange, L. E. Cadus, *J. Catal.* **2005**, *231*, 232-244; c) S. Royer, F. Berube, S. Kaliaguine, *Appl. Catal. A:General* **2005**, *282*, 273-284.

[39] G. L. Chiarello, J. D. Grunwald, D. Ferri, F. Krumeich, C. Oliva, L. Forni, A. Baiker, *J. Catal.* **2007**, *252*, 127-136.

[40] N. Tien-Thao, H. Alamdari, M. H. Zahedi-Niaki, S. Kaliaguine, *Appl. Catal. A:General* **2006**, *311*, 204-212.

[41] J. A. Dalmon, P. Chaumette, C. Mirodatos, *Catal. Today* **1992**, *15*, 101-127.

[42] A. J. Marchi, J. I. DiCosimo, C. R. Apesteguía, *Catal. Today* **1992**, *15*, 383-394.

[43] D. Ferri, A. Heel, D. Burnat, in *Perovskites and related mixed oxides: concepts and applications*, 1st ed. (Eds.: P. Granger, V. I. Parvulescu, S. Kaliaguine, W. Prellier), Wiley-VCH Verlag GmbH & Co. KGaA, **2016**, p. 69.

[44] P. Malet, A. Caballero, *J. Chem. Soc., Faraday Trans. I* **1988**, *84*, 2369-2375.

[45] B. Ravel, M. Newville, *Journal of Synchrotron Radiation* **2005**, *12*, 537-541.

10.1002/cphc.201800069

WILEY-VCH

ARTICLE

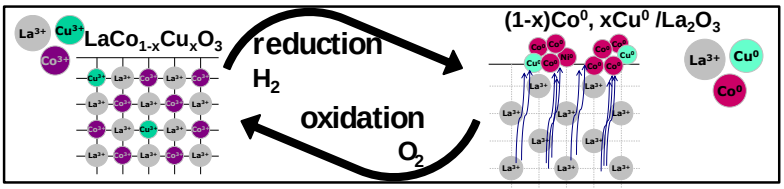

Reversible structures: The cations (Co^{3+},Cu^{3+}) inserted on B-site of the perovskite can be reduced by forming metallic particles on the surface of the resulting La_2O_3. After an oxidative treatment, the Co and/or Cu particles go back inside the structure lattice, regenerating the perovskite.